NUMERICAL ANALYSIS OF THE INTERACTION OF PARTICLE FLOWS WITH THE VORTEX DYNAMICS IN A DOUBLE EXPANSION

Allan LOVE[1*], Donald GIDDINGS and Henry POWER

[1]Energy and Sustainability Division, The University of Nottingham, Nottingham, UNITED KINGDOM
*Corresponding author, E-mail address: enxail@nottingham.ac.uk

ABSTRACT

The dispersion of solid particles within flows having zones of recirculation is of interest in pulverised fuel distribution and combustion at burners. Previous modelling of a ¼ scale test rig was performed by Giddings et al. (2004), and an instability later identified within the domain. Subsequently the transient dynamics of the flow of air through a double expansion were investigated numerically and a recirculation zone was found to develop at one of the four corners of the expansion. In the work presented here the flow of solid particles through this double expansion is investigated using the commercial software ANSYS FLUENT. The Stress-Omega Reynolds Stress Model is used to model the gas phase turbulence and the Discrete Particle Modelling approach is used to model the solid particle flow. The dynamics of the flow are reported here for 10µm and 60µm particles at a mass loading of 0.07. The simulations show a distinct transition to a vortex shedding type instability with the addition of the discrete phase.

NOMENCLATURE

B downstream duct height, m
D_D downstream duct width, m
D_p particle diameter, m
D inlet diameter, m
F_D drag force
g gravitational acceleration
t time
x x-axis
y y-axis
z z-axis
u_p particle velocity
u_g continuous phase velocity
U x-axis Reynolds-averaged velocity component, m.s^{-1}
V y-axis Reynolds-averaged velocity component, m.s^{-1}
W z-axis Reynolds-averaged velocity component, m.s^{-}
Re Reynolds number based on D

St Stokes number ($St = \dfrac{\rho_p D_p^2 V}{18\mu D}$)

ρ density, kg.m^{-3}
μ dynamic viscosity, kg m^{-1}s^{-1}

INTRODUCTION

The steady pneumatic transport of solid particles is of importance to many industries. This is particularly true of coal fired power plants where coal is first ground in the mills before being pneumatically transported to a number of burners through a convoluted system of pipes and splitters. In order to ensure good performance a steady homogenous supply of fuel to the burners is desirable. This is difficult to achieve due to the inertia of the particles and their tendency to form 'ropes' at bends. The presence of other flow features, such as separation and formation of a recirculation zone at expansions within this piping system, further complicates the picture. The study by Kuan and Yang (2005) highlighted the unsteady flow downstream of a bifurcation. In addition, the interaction of pulverised fuel with a recirculation is key to the stability and NO$_x$ performance of low NO$_x$ burners.

In this study the flow through a double expansion is investigated. There are a number of examples in the literature of flow through circular-to-rectangular transition ducts (Patrick and McCormick, 1988; Miau et al., 1990; Davis and Gessner, 1992). Patrick and McCormick (1988) found asymmetric flow within a circular-to-rectangular transition duct. Miau et al. (1990) went on to investigated the flow field in three transition ducts of constant cross sectional area with different lengths over a range of turbulent Reynolds numbers. A separation bubble, or stall region, was found in one corner for the lowest Reynolds number case, disappearing at higher Reynolds numbers. Characteristics of the flow depended primarily on the geometry. Diffuser geometries do not maintain a constant cross sectional area and can expand in two or three dimensions. Therefore, a greater adverse pressure gradient is present and boundary layer separation is more likely. Turbulent flow through planar two dimensional diffusers generates a number of flow regimes (Fox and Kline, 1962). The transitory stall regime is characterised by the formation of a large recirculation in one corner.

The dispersion of particles at a recirculation downstream of backward facing step was investigated by Hardalupas et al. (1992). Particles only enter the recirculation zone due to turbulent dispersion as they must cross the dividing stream line. They found bimodal probability distribution functions for both axial and inclined velocities near the shear layer for a large eddy stokes number of 1. Particle concentration in the recirculation zone increased abruptly for a Stokes number of 1. Eaton and Fessler (1994) provide an overview of preferential particle concentration by turbulence. It has been shown for many flows that small particles concentrate on the outside and between coherent vortex structures. Meiburg et al. (2000) modelled the fluid vorticity field for particle laden mixing layers using a Eulerian-Lagrangian approach including two-way coupling. For the case of differential particle loading between two streams a direct shift was observed in the Kelvin-Helmholtz vortex towards the seeded stream

compared to the uniform particle distribution case. This was due to an increase in vorticity generation on the side of the seeded stream.

Previous modelling of a ¼ scale test rig, resembling a section of a pulverised fuel piping system, was performed by Giddings et al. (2004). An instability was later identified within the domain. Within the geometry of the bifurcator a recirculation zone became established and it was observed that the interaction of the particle phase with this recirculation zone made a satisfactory steady state solution impossible. Subsequently the transient dynamics of the flow through a double expansion have been investigated numerically and a recirculation zone was found to develop at one of the four corners of the expansion, together with evidence of a precessing motion of the jet. The present study examines the effects of the particles on this flow field. The commercial CFD code ANSYS FLUENT 14.0 is used. The dynamics of the flow are investigated for 10μm and 60μm particles for a mass loading of 0.07.

MODEL DESCRIPTION

Geometry Model and Mesh

The modelled geometry was originally adapted from the bifurcator of Giddings et al. (2004). For the case of a straight inlet, attached to this geometry, a recirculation zone developed in each of the four corners, but larger recirculation zones formed in two opposing corners of the four. The two large recirculation zones were thought to be an outlet condition effect and so the flow has been studied with the bifurcator outlets removed.

This resulted in the diffuser geometry with two expansions: the first being 3D and the second 2D. Dimensions of the geometry are shown in Fig.1. A fully three dimensional structured grid has been used (Fig.2), with an O-grid used throughout and care taken to ensure orthogonality and a smooth variation of the cell structure across the domain. The cell density along the axis is non-uniform with neighbouring cells varying in size by no more than 10%. y^+ was close to 30 throughout the domain. A mesh of 600,000 cells picked up distinct frequencies for the oscillating velocity fields for the Re=170,000 air flow case. The mesh was refined by 50% in all directions and this yielded a similar result for the main oscillating frequency (Table 1). On a 50% coarser mesh, the magnitude of all oscillations was reduced, and no distinct frequencies were visible. Comparisons of velocity profiles for each mesh showed minimal variation.

Gas Phase

Isothermal simulations were performed using the commercial CFD package ANSYS FLUENT 14.0, which solves the Navier Stokes Equations using the finite volume method. Turbulence was modelled using the Stress-Omega Reynolds Stress Model (RSM) with shear flow corrections applied. Previous studies have determined RSMs to be the most capable RANS models for representing the flow topography in 3D diffuser flows (Steiner et al. 2008 and Karvinen and Ahlstedt (2008)). Berdanier, (2001) compare the RSM Stress Omega formulation with other RANS models, noting that it gave the best representation of the recirculation region in a 2D diffuser.

The pressure based solver was used. The PISO algorithm was used for pressure correction. The convective and diffusion terms were represented using a second order upwind scheme. Time discretisation was achieved using the first order fully implicit scheme. The equation solver used was Alegbraic Multigrid.

Mesh (cells)	Precessing Frequency (Hz)	Recirculation Length (m)
300k	NA	1.16
600k	4.6	1.2
1,200k	4.6	1.18

Table 1: Results for different mesh resolutions.
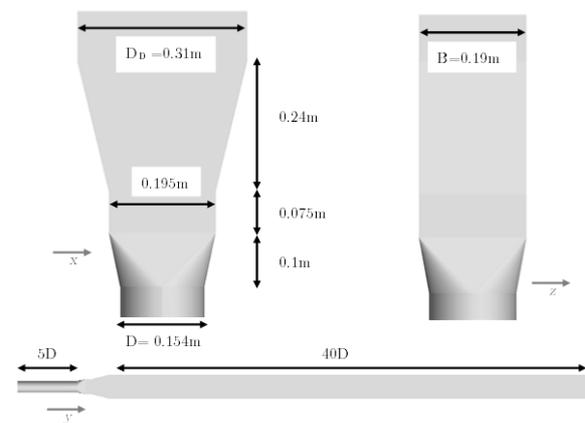
Figure 1: Dimensions of the diffuser.
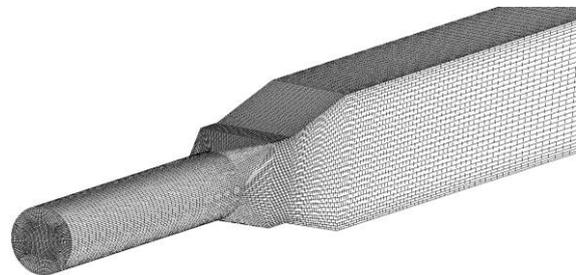
Figure 2: A typical mesh used in the calculations.

Transient solutions were initialized from the steady state case, but the final solutions were independent of these initial solutions. The time step used was 2.5×10^{-4}s with a maximum Courant number of 1.8. Further reduction in the time step did not significantly change the flow characteristics. Gravity was defined in the y-direction as 9.81ms^{-2}.

Convergence, for the air flow case, was judged based on the global sum of the residuals for the main flow variables and equations, which were allowed to approach the accuracy for single precision. The mass balance between the inlet and outlet of the domain was also monitored to ensure continuity. Finally, the velocity and pressure were monitored at various points until the frequency and magnitude of the oscillations did not change with further iteration. (Convergence for the particle phase was judged

in the same way, however, the global sum of the residuals was judged to have converged for scaled values of 10^{-4} or less). For each mass loading atleast 2000 timesteps (0.5 seconds) were simulated. After an initial settling period, no significant changes in the results were observed.

Particle-Phase

The discrete phase was modelled as glass cenospheres ($\rho=700$ kg m^{-3}). Results for two particle sizes, 10 and 60 μm (St=0.02 and 0.78 respectively), at a mass loading of 0.07 are shown. The particle phase was modelled using the Lagrangian approach with FLUENT's Discrete Particle Model. Here the Lagrangian tracking method is used to solve the individual trajectories of the theoretical particles by equating their inertia with external forces:

$$\frac{du_p}{dt} = F_D(u_p - u_g) + \frac{g(\rho_p - \rho_g)}{\rho_p} \qquad (1)$$

The drag force is determined by the spherical drag law of Morsi and Alexander (ANSYS, 2011). The gravity force is determined from the density difference between the particle and the fluid. Two-way coupling, exchange of momentum between the particles and fluid, was accounted for. Additional forces, such as Saffman lift force and virtual mass force were not accounted for in this work.

The presence of the recirculation and shear layer, results in concentration of the particles in this region and particle dispersion may be enhanced by treatment of collisions at higher mass loadings. For the results reported the particle volume fractions are typically <0.001 (Elghohbashi, 1994) and so a stochastic collision model has not been included in this study.

The discrete random walk model has been used to model the effect of fluid turbulence on the particle path. 5 random tries were defined for each inlet. In total 18,000 particles tracks were modelled. While the continuous phase is modelled as time dependent, the particles have been treated as steady.

Boundary Conditions

The inflow boundary condition was specified 25D upstream of the diffuser as a fully developed velocity profile parallel to the pipe axis. A characteristic length based on the inlet pipe diameter and an estimate of turbulence intensity was also defined. The theoretical particle tracks were injected from the inlet surface with a velocity of 90% of the bulk velocity (14.4ms^{-1}) and were suitably dispersed upon reaching the diffuser. A pressure outlet condition was used for the outflow. The outlet duct length of 40D was determined sufficient to not affect the flow at the diffuser. The reference pressure was set as atmospheric, where the pressure drop through the geometry was only 160 Pa. The heights of the near wall cells were sufficient to accurately represent the boundary layer in each case.

On the wall surfaces a no slip boundary condition was defined for the fluid. Much work has been done on the interaction of particles with the wall (Sommerfeld 1999, Kuan et al. 2007) and while it is acknowledge that this is a function of wall roughness, impact angle and material properties, the particle wall interaction was modelled using a constant restitution coefficient of 0.9 in this study.

Initial Conditions

The transient cases were initialized from the corresponding steady state case. It was observed that for both the steady state and transient cases the flow developed in the same way. The dispersed phase was injected into the fully converged air flow field. The mass loading of the discrete phase was ramped up slowly.

RESULTS

Air flow field characteristics

A previous numerical investigation of the air flow case established the flow topography over a range of Reynolds numbers (Love et al. 2012). For Re>80,000 one large recirculation became established within one corner of the diffuser. Upon reducing the flowrate, for Re<80,000 greater separation took place, and the flow field was more chaotic (Fig. 3). This transition has been attributed to the Coanda effect, or the jets ability to entrain fluid at higher flowrates (Panitz and Wasan (1972)). For a jet close to a wall the volume of fluid which can be entrained is limited, leading to the formation of a low pressure region and thus the jet deflects and becomes permanently attached to the wall. For a symmetrical 2D diffuser, Chiekh et al. (2003) observed two stable states illustrating this phenomenon, where the flow was both deflected and attached to the top or bottom wall. This formation of a lone recirculation zone in one corner is consistent with the circular-to-transition ducts of Miau et al. (1990) and 2D and 3D diffuser geometries of Fox and Kline (1962) and Steiner et al. (2008). This flow field is reasonably steady, and the only instability being a small scale precession motion of the jet with characteristic frequency (Love et al. 2012).

Effect of the dispersed phase

The discrete phase was investigated for monodispersed particles of sizes 10μm and 60μm. The particle flow field is investigated for an air inlet velocity of 16ms^{-1} (Re=170,000). It was found that even small mass loadings had a significant effect on the flow field. The results for a mass loading of 0.07 are reported.

Figure 4 shows a comparison of the instantaneous axial velocity profiles, for the diagonal across traversing the recirculation zone, for the continuous phase. The addition of particles moves the maximum axial velocity closer to the centre of the diffuser. This can be attributed to the increased momentum of the main flow. Despite this the airflow and 10μm particle case bear a close resemblance, as would be expected given the low particle Stokes number. For higher particle stokes numbers and mass loading, it is expected that greater separation will occur due to the increased momentum of the main flow. For the 60μm particle case the length of the recirculation zone is shorter (this is true for all time steps). The length of the large recirculation zone is just ~0.95m in this case compared to ~1.16m for the air and 10μm particle cases. This may only be partly explained by the formation of a small recirculation in the opposing corner.

    (a) Re=170,000   (b) Re=80,000   (c) Re=42,000
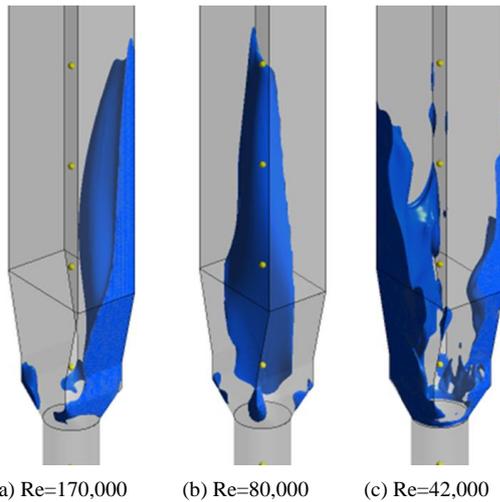
Figure 3: Flow topography, highlighting the recirculation zone, shown by axial velocity contours of $-0.01 \mathrm{ms}^{-1}$.
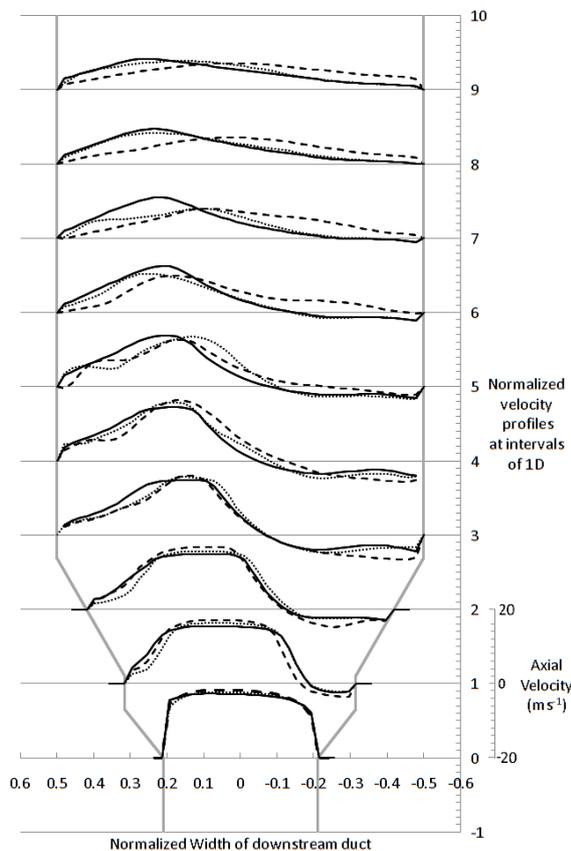
Figure 4: Normalized instantaneous air velocity profiles for air (-), 10μm (...) and 60μm (--) particles cases.

Figure 5 compares vorticity contours for a diagonal plane through the recirculation zone. It is immediately obvious that for the particle cases, large scale coherent vortex structures are forming. These travel downstream and are subsequently shed as shown in Fig. 6. In all cases the vorticity at the entrance to the diffuser is high due to the curvature of the flow field and development of the shear layers. Small but significant differences can be seen between each case. For the 60μm it can be seen that the vorticity is higher along main shear layer. Whereas, for the 10μm particle case the vorticity is noticeably higher close to the shear layer of the opposing, smaller recirculation. In both cases, the generation of vorticity by the particle laden jet initiates the vortex shedding. This is the mechanism discussed by Meiburg et al. (2002). This is similar to the Kelvin-Helmholtz instability between stratified layers of different density, as the particle stream effectively increases the density of the main flow. The generation of vorticity leads to larger coherent structures. For the 60μm particle case, these structures are large and thus entrain more of the surrounding fluid, leading to the reduction in the size of the recirculation, described above. This same effect is likely to be the cause of the instability for our bifurcator work mentioned previously and explains the difficulty in achieving a satisfactory steady state solution.

Figure 7 shows a comparison of contours of particle concentration. It can be seen that the particles concentrate on main flow side of the shear layer. This concentration effect is both an effect of the curvature of the main flow field and recirculation of the particles. The recirculated particles are slower moving and concentrate at the bottom of the recirculation before re-entering the main flow field. For both cases the concentration of particles within the recirculation is relatively low.

From looking at the spread of particle axial velocities it is clear that the majority negative particle velocities occur in the largest recirculation. This allows the cumulative velocity histograms across a horizontal plane to be used as an indicator of the mass of the discrete phase entering the main recirculation. In both the 60μm and 10μm cases the peak is about 12% of the total mass loading, occurring between 2 and 4D downstream of the diffuser entrance. The 60um particle case adds mass rapidly near the top of the recirculation zone and loses it rapidly at 1D. Whereas, particles are entrained more gradually in the 10μm case. In addition, particle tracks indicate that it is the coherent vortex structures which are responsible for particle dispersion into the recirculation zone. Figure 8 and 9 show the particle velocities at various downstream distances. It can be seen that as expected the particles largely follow the gas flow field. However, there is evidence of greater variation in particle axial velocities due to interaction with vortices in the shear layer (at 5 and 7D in both cases). This would agree with the work of Hardalupas et al. (1992) who found a bimodal particle velocity distribution near the shear layer for the axisymmetric backward facing step flow.

Furthermore, it can be seen that the particle phase also concentrates in the corner opposite the main recirculation. The secondary velocities (those not in the streamwise direction) will pull the particles towards this corner. In the corner regions the velocity of the air flow is reduced due to high shear. In the 10μm particle case there is also an increase in vorticity in this region. This leads to a decrease in particle velocity and an increase in particle concentration, and the secondary peaks shown in the velocity profiles.

CONCLUSIONS

The air and particle flows through a double expansion have been investigated. This was prompted to explain flow asymmetries and instability within a bifurcator geometry. This work is relevant to the pneumatic

conveying of pulverised fuel, where transitions in pipe geometry are common, and instabilities can affect steady flow. For the air flow case the formation of one large recirculation within one corner of the geometry has been observed and this is attributed to the Coanda effect. The addition of particles at a small mass loading leads to a significant change in the flow dynamics. The simulated particles increased the vorticity at the shear layer and lead to the formation and shedding of coherent vortex structures. Despite a low mass loading both phases are closely coupled. Particle concentration was highest at the beginning of the shear layer and in the opposing corner to the main recirculation. Particles appear to enter the recirculation through dispersion by interaction with the vortices in the shear layer.

Future work will focus on further characterisation of the flow at higher mass loadings. It is anticipated that for increased mass loading and higher particle stokes numbers greater separation will occur within the flow field. In addition, the effect of gravity on the recirculating flow will be investigated.

ACKNOWLEDGEMENTS

REFERENCES

ANSYS (2011), "FLUENT User's Guide", ANSYS, Inc. Release 14.0

BERDANIER, R. A. (2011). "Turbulent flow through an asymmetric plane diffuser". *Masters, Purdue University*.

CHIEKH, M. B., BERA, J.-C., and SUNYACH, M. (2003), "Synthetic jet control for flows in", *Journal of Turbulence*, **4(32)**, 37–41.

DAVIS, D. O. and GESSNER, F. B., (1992), "Experimental investigation of turbulent flow through a circular-to-rectangular transition duct.", *AIAA Journal1*, **30(2)**, 367 – 375.

EATON, J.K. and FESSLER, J.R., (1994), "Preferential concentration of particle by turbulence", *Int. J. Multiphase Flow,* **20**, 169-209

FOX, R. W. and KLINE, S. J., (1962), "Flow Regimes in Curved Subsonic Diffusers", *Journal of Basic Engineering*, **84(3)**, 303–312.

GIDDINGS, D., AROUSSI, A., PICKERING, S., and MOZAFFARI, E., (2004), "A 1/4 scale test facility for PF transport in power station pipelines." Fuel, 83(16):2195–2204.
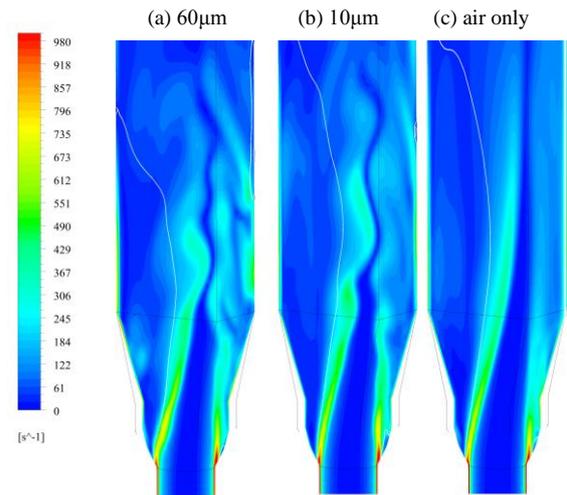
Figure 5: Vorticity contours (s^{-1}). Recirculation zone shown by white contour of axial velocity -0.01ms^{-1}.
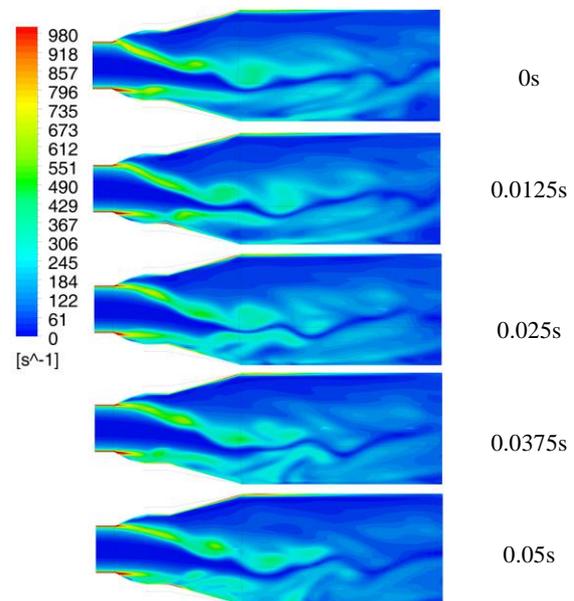
Figure 6: Development of vorticity field with time for 60μm particle case.
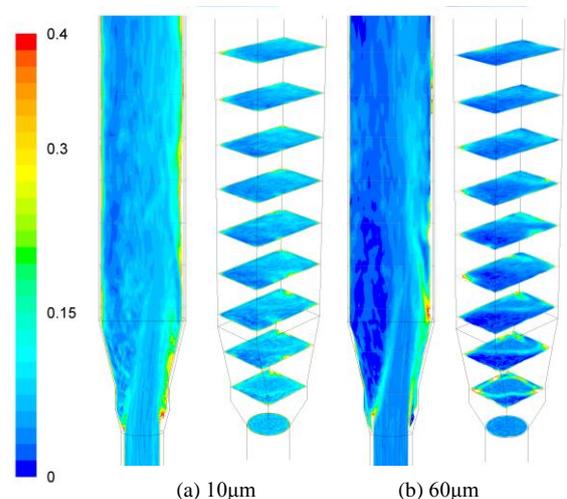
Figure 7: Comparison of particle concentration (kg m^{-3})

HARDALUPAS, Y., TAYLOR, A.M.K.P. AND WHITELAW, J.H., (1992), "Particle dispersion in a vertical round sudden-expansion flow", *Phil. Trans. R. Soc. Lond. A.*, **341,** 411-442

KARVINEN, A. and AHLSTEDT, H. (2008), "Comparison of turbulence models in case of three-dimensional diffuser", *In Proceedings*
of Open Source CFD International Conference
 2008, number 2008.

KUAN, B., REA, N., and SCHWARZ, P, (2007), "Application of CFD in the design of a grit collection system for the coal-fired power generation industry", *Powder technology*, **179**, 65-72

KUAN, B., and YANG, W., (2005), "Mal-distribution of coals in lignite-fired power station mill ducts: CFD simulations and experimental validation", *International conference on coal science and technology 2005,*Okiinawa

LOVE, A., GIDDINGS, D., POWER, H., (2012), "Numerical analysis of vortex dynamics in a double expansion", *to be submitted.*

MEIBURG, E., WALLNER, E., PAGELLA, A., RIAZ, A. HARTEL, C. AND NECHER, F. (2000), "Vorticity dynamics of dilute two-way-coupled particle-laden mixing layers", *J. Fluid Mech.*, **421**, 185-227

MIAU, J. J., LEU, T. S., CHOU, J. H., LIN, S. A., and LIN, C. (1990), "Flow distortion in a circular-to-rectangular transition Duct", *AIAA Journal*, **28(8)**,1447 – 1456.

PANITZ, T. and WASAN, D. T. (1972), "Flow attachment to solid surfaces: The Coanda effect", *AIChE Journal*, **18(1)**, 51–57

PATRICK, W. P. and MCCORMICK, D. C. (1988), "Laser Velocimeter and Total Pressure Measurements in Circular-to-Rectangular Transition Ducts", Technical Report 87, United Technologies Research Center.

SOMMERFELD, M. and HUBER, N., (1999), "Experimental analysis and modelling of particle-wall collisions", *International Journal of Multiphase Flow,* **25,** 1457-1489

STEINER, H., JAKIRLIC, S., KADAVELIL, G., MANCEAU, R., SARIC, S., and BRENN, G. (2008), *13th ERCOFTAC Workshop on*
Refined Turbulence Modelling. ERCOFTAC Bulletin **78**, 22–27.
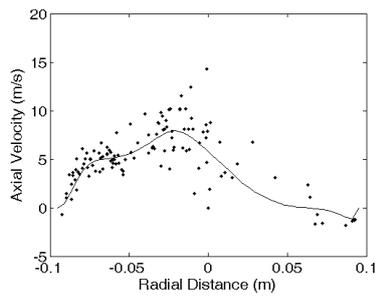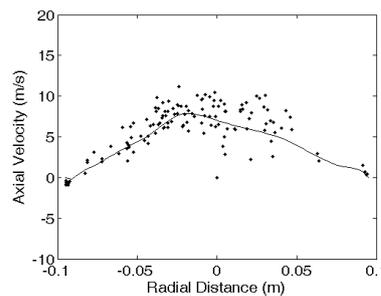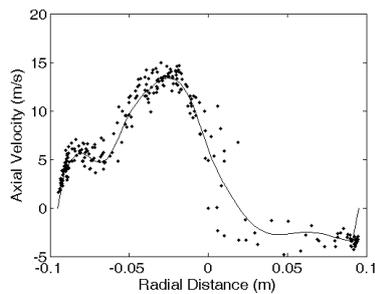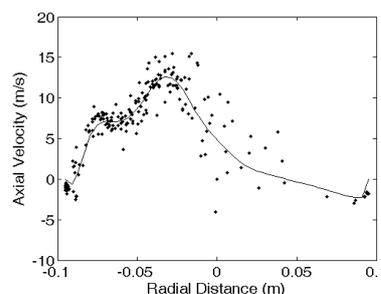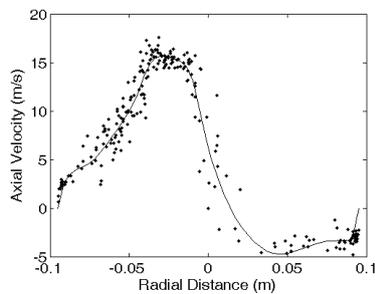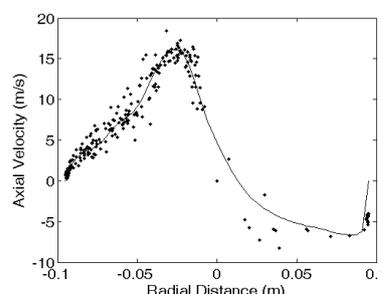
Figure 5: Comparison of continuous phase velocity profile (-) and 10μm particle velocities (.).

Figure 6: Comparison of continuous phase velocity profile (-) and 60μm particle velocities (.).